Applied Catalysis B: Environmental 248 (2019) 459–465

Contents lists available at ScienceDirect

Applied Catalysis B: Environmental

journal homepage: www.elsevier.com/locate/apcatb

In-situ fabrication of atomic charge transferring path for constructing heterojunction photocatalysts with hierarchical structure

Dongxu Liu[a], Jing Zhang[a,*], Chun Li[a], Xun Zhang[a], Xuebing Chen[a], Fangfang Wang[a], Ming Shi[b], Rengui Li[b,*], Can Li[b]

[a] College of Chemistry, Chemical Engineering and Environmental Engineering, Liaoning Shihua University, Fushun 113001, Liaoning, China
[b] State Key Laboratory of Catalysis, Dalian Institute of Chemical Physics, Chinese Academy of Sciences, Dalian 116023, Liaoning, China

ARTICLE INFO

Keywords:
Charge separation
Heterojunction
Photocatalysis
Hierarchical structure

ABSTRACT

The efficiencies of photocatalytic solar energy conversion systems are significantly limited by the challenging charge separation process, which can be improved via some commonly-used interfacial modulating strategies, e.g., introducing heterojunctions at the interfaces of different semiconductors. However, in many cases, the constructed heterojunctions not always work well mainly due to the serious mismatching of surface and energy structures between different components. In this study, inspired by the similarities in crystalline structures and elemental compositions, a novel heterojunction photocatalyst with hierarchical structure was first fabricated between bismuth-based semiconductors ($Bi_2Ti_2O_7$ and γ-Bi_2O_3) possessing identical cubic phase via a simple in-situ transformation method. The resulted $Bi_2Ti_2O_7$/γ-Bi_2O_3 heterojunction photocatalyst (denoted as BT/γ-Bi_2O_3) shows extremely high photocatalytic activities in photocatalytic removal of various high concentration environmental pollutants, e.g., phenol, dyes and sulfur containing compounds. An enhancement of more than two orders of magnitude in photocatalytic performances can be achieved for the BT/γ-Bi_2O_3 photocatalyst than the single composite, which is possibly attributable to the co-sharing of Bi-O tetrahedra units for the composites in heterojunction structures to provide an atomic charge transferring pathway for facilitating the spatial charge separation. This work provides an effective strategy for rationally constructing charge separation and transfer pathway in semiconductor-based photocatalysts for solar energy conversion.

1. Introduction

The efficiencies of photocatalytic solar energy conversion systems are significantly determined by the challenging charge separation process, which is regarded as a bottleneck and critical issue in the field of photocatalysis [1–4]. Among the strategies to boost spatial charge separation and inhibit charge recombination, heterojunction strategies are demonstrated to be able to facilitate spatial charge separation originated from driven force providing by the built-in electric field at the heterojunction region [5–9]. Heterojunctions, in general, are fabricated as the interface of different semiconductors possessing different band structures and Femi levels to satisfy the thermal-dynamical requirement, which is a prerequisite for inducing the interfacial band alignments [10–13]. Nevertheless, the efficient charge separation at heterojunction region requires not only the suitable band alignment, but also determines by many other key factors, e.g., well-defined interfacial structures with less mismatching in junction region, which can minimize the energy barrier at the interface so that the photogenerated electrons and holes can smoothly migrate to the opposite sites for desired redox photoreactions [14,15]. This is the reason why the constructed heterojunctions not always work well in some cases because of the serious mismatching of interfacial structures between different components in atomic level.

Interfacial mismatching at the heterojunction region is intrinsically caused by the differentiated crystalline structures between different components and also inappropriate preparation methods [16,17]. When the two semiconductors possess very similar crystalline structures and elemental framework, together with suitable band aliments, they will be promising to be acting as perfect candidates to construct a heterojunction structure between them for efficient charge separation. Meanwhile, In-situ fabrication of a heterojunction structure between two components is also essentially importance for forming a compact interfacial pathway to promote the fast migration of charge carriers at the interface [18,19].

Bismuth-based semiconductors are a class of unique and promising materials in energy and environmental fields, e.g., Bi_2O_3, Bi_2MO_6

* Corresponding authors.
E-mail addresses: zhangjing@lnpu.edu.cn (J. Zhang), rgli@lnpu.edu.cn (R. Li).

https://doi.org/10.1016/j.apcatb.2019.02.050
Received 20 September 2018; Received in revised form 9 January 2019; Accepted 18 February 2019
Available online 19 February 2019
0926-3373/

(M = Cr, Mo and W), $BiVO_4$, BiOX (X = Cl, Br and I), $BiPO_4$, $(BiO)_2CO_3$, and pentavalent bismuthates [20–28]. The electronic structures of bismuth-based semiconductors confer them with suitable band gaps for visible-light response and well-dispersed valence bands composed of hybrid orbitals of Bi_{6s} and O_{2p}, making them a promising candidate when compared to other metal oxide semiconductors [29]. One of the most important points is that almost all of these bismuth-based semiconductors contain specific Bi-O tetrahedra units in their crystalline structure, which consequently correlates to their superior physiochemical properties. Together considering the merits of heterojunction and the unique structures of bismuth-based semiconductors, it is desirable to construct a perfect heterojunction between two bismuth-based semiconductors with very similar crystalline structures.

In this work, based on the analyzing of similarities in crystalline and energy structures for various bismuth-based semiconductors, a novel heterojunction photocatalyst with hierarchical structure was first fabricated between two bismuth-containing semiconductors ($Bi_2Ti_2O_7$ and γ-Bi_2O_3) possessing identical cubic phase via a simple in-situ transformation method. We found that the resulted $Bi_2Ti_2O_7$/γ-Bi_2O_3 heterojunction photocatalyst (denoted as BT/γ-Bi_2O_3) shows extremely high photocatalytic activities in photocatalytic removal of various high concentration environmental pollutants, e.g., phenol, dyes, and sulfur containing compounds. An enhancement of more than two orders of magnitude in photocatalytic performances can be achieved for the BT/γ-Bi_2O_3 photocatalyst than the single composite, which is due to the co-sharing of Bi-O tetrahedra units for both composites in heterojunction structures to provide an atomic charge transferring pathway for spatial charge separation.

2. Experimental section

2.1. Materials

Bismuth nitrate pentahydrate ($Bi(NO_3)_3{\cdot}5H_2O$), tetrabutyl titanate (TBOT, $Ti[O(CH_2)_3CH_3]_4$), anhydrous ethanol, glycol, sodium hydroxide (NaOH), disodium ethylenediaminetetraacetate (EDTA), methanol, ascorbic acid, dibenzothiophene (DBT, 98%), and dodecane (99%) used in this work were of analytical grade without further purification. Distilled water was used throughout.

2.2. Sample preparation

2.2.1. Synthesis of γ-Bi_2O_3

In a typical procedure, 5 g of $Bi(NO_3)_3{\cdot}5H_2O$ was dissolved in 20 ml of HNO_3 (1 mol L^{-1}) to avoid hydrolyzation of Bi^{3+} ions. A 2 mol L^{-1} NaOH solution was stirred at 75 °C while the above $Bi(NO_3)_3$ solution (0.5 mol L^{-1}) was slowly added. After reaction time of 6 h, the resulting precipitate was washed with deionized water and anhydrous ethanol several times and subsequently dried at 60 °C overnight. The obtained samples were labeled as γ-Bi_2O_3.

2.2.2. Synthesis of $Bi_2Ti_2O_7$/γ-Bi_2O_3 composites

The above γ-Bi_2O_3 sample was used as a support for BT/γ-Bi_2O_3. A certain amount of TBOT was dissolved in mixed solution of glycol and ethanol (volume ratio is 2:1). The γ-Bi_2O_3 support was impregnated with the above mixed solution, and subsequently stirred in a hot water bath until it was dried. After the sample was kept at 110 °C overnight, it was calcined at 500 °C in air for 2 h. The obtained samples are denoted as n% BT/γ-Bi_2O_3, where n represents the mass ratio of Ti and Bi.

2.3. Characterization

X-ray Powder Diffraction (XRD) patterns were obtained on a Rigaku MiniFlex diffractometer with a Cu Kα radiation source. SEM (EDS) images were taken with Quanta 200 FEG scanning electron microscope. UV–vis diffuse reflectance spectra (UV–vis DRS) were recorded on a JASCO V-650 UV–vis spectrophotometer. Nitrogen adsorption isotherm of the sample was measured on a gas sorption analyzer (ASAP 2000 automated BET surface area) at 77 K using liquid nitrogen. The sample was degassed at 300 °C for 3 h before BET measurement. The surface area was calculated by the BET equation. Raman spectra were measured at room temperature with a home-assembled Raman triple-stage spectrograph with spectral resolution of 2 cm^{-1} (DL-3 UV Raman spectroscopy with operando system). The line at 532 nm from a MGL-III-532-200 mW laser (Changchun New Industrial Optoelectronics Tech Co.) was used as the excitation source.

2.4. Photocatalytic activity for degradation of dye, phenol, and sulfur containing compounds

Photocatalytic degradation of organic dye or phenol pollutants was carried out in 100 mL Pyrex reactor filled with ion-exchanged water (60 mL) containing 4-chlorophenol (20 mg/L) (20 mg/L RhB or 20 mg/L methyl orange) and 60 mg BT/γ-Bi_2O_3 samples. Before illumination, adsorption-desorption equilibrium of 4-chlorophenol (RhB or methyl orange) on the catalyst was obtained by stirring the suspension in the dark for 30 min. The suspension was placed under and kept 15 cm distance away from a 300 W xenon (Xe) lamp (PLS-SXE300, Beijing Perfect Light Co., China), and the irradiation power of Xe lamp at solution level is 192.4 mW/cm^2. Sampling was taken every certain time after irradiation. 3 mL aliquot was centrifuged, and the obtained clear solution was analyzed by the optical characteristic absorption (UV mini 1240 spectrophotometer, Shimadzu Corporation). The degree of mineralization was monitored through analysis of the total organic carbon (TOC) content in the irradiated solution using a SHIMADZU TOC-VSCH analyzer. The experiments without xenon lamp and without catalysts were performed as blank experiments. The stability of BT/γ-Bi_2O_3, a typical catalyst in this study, was examined by three cycles in photocatalytic degradation of 20 mg/L Rhodamine B or 4-chlorophenol. Before each cycle the catalyst was recycled and washed by deionized water.

The photocatalytic oxidative desulfurization (PODS) of dibenzothiophene (DBT) is evaluated within a dodecane/methanol biphasic system in the presence of H_2O_2 as an oxidizing reagent. The model fuel with a sulfur concentration of 200 mg/L was prepared by dissolving DBT in dodecane. PODS reaction was carried out in 100 mL Pyrex reactor filled with 20 mL of model fuel and 20 mL methanol containing hydrogen peroxide (O/S mole ratio = 30:1) and 0.12 g photocatalyst. The distance between the Xe light source and the surface of the reaction solution is 15 cm and the irradiation power of Xe lamp at solution level is 192.4 mW/cm^2. Prior to the catalytic reaction, the suspension was magnetic stirring for 30 min to ensure an adsorption-desorption equilibration of the system. At settled intervals, a 2 mL upper layer solution was taken with an interval of 30 min and immediately centrifuged. The upper clear solution was subjected to sulfur measurement by a WK-2D type microcoulomb comprehensive analyzer. The operating parameter was followed by integral resistance 400 Ω, bias voltage between 148 and 149 mV, burning furnace temperature 850 °C, evaporation section temperature 750 °C, and stable section temperature 650 °C, the oxygen flow rate 150 mL min^{-1} and nitrogen flow rate 260 mL min^{-1}. The desulfurization rate of model fuel (η) was calculated by the Eq. (1):

$$\eta = \left(1 - \frac{C}{C_0}\right) \times 100\% \quad (1)$$

where C_o is the sulfur content of the feed, and C is the sulfur content of the product after photocatalytic reaction.

2.5. Active species trapping experiments

In our work, disodium ethylenediaminetetraacetate (EDTA),

methanol, and the ascorbic acid was added in the photocatalytic degradation of RhB or 4-CP to investigate the main active species, such as remove hole (h^+), hydroxyl radical ($^{\cdot}OH$), and superoxide radical ($^{\cdot}O_2^-$) [30–33]. The amount of EDTA, methanol, and the ascorbic acid was 10 mmol. The other experimental conditions were kept the same as the photocatalytic activity test in Section 2.4.

2.6. Photoelectrochemical measurements

The photocurrents, electrochemical impedance spectra (EIS), and Mott-Schottky curves were measured on an electrochemical workstation (Ivium Vertex One) and carried out in a three-electrode system with a working electrode, Ag/AgCl (saturated KCl) as the reference electrode, Pt plate as the counter electrode. 0.1 M Na_2SO_4 was used as the electrolyte solution. A 300 W Xe lamp (Beijing Perfect Light Co., China) was used as the light source. The working electrode was prepared by dip-coating BT/γ-Bi_2O_3 or γ-Bi_2O_3 slurry on an F-doped tin oxide (FTO) glass electrode (2 cm × 0.5 cm) and dried at room temperature for 12 h. The Mott-Schottky measurements were conducted from 1 to −1 V vs. Ag/AgCl at 1000 Hz. The photocurrent responses of the samples were measured at linear sweeping voltammetry from −0.1 V to 1 V. the frequency was scanned from 100 kHz to 100 mHz, and the electrolyte was 0.1 M $K_3Fe(CN)_6/K_4Fe(CN)_6$ (1/1) and 0.1 M Na_2SO_4.

3. Results and discussions

γ-Bi_2O_3 is the cubic phase bismuth compound with a band gap of 2.8 eV, making it a viable visible-light-responsive photocatalyst. By analyzing the crystalline and energy structures of γ-Bi_2O_3 with other bismuth-based semiconductors, another promising semiconductor that is $Bi_2Ti_2O_7$ attracts our attention. $Bi_2Ti_2O_7$ belongs to a family of $A_2B_2O_7$ compounds with its crystal structures were comprised of Ti-O octahedra units and Bi-O tetrahedra units. Except for the co-containing of Bi-O tetrahedra units, the crystal lattices of γ-Bi_2O_3 and $Bi_2Ti_2O_7$ are in cubic symmetry and the lattice dimensions are almost the same, e.g., 10.25 Å and 10.37 Å for γ-Bi_2O_3 and $Bi_2Ti_2O_7$, respectively [34]. These factors offer the possibility of in-situ transformation of $Bi_2Ti_2O_7$ by introducing Ti atoms in the bulk structure of γ-Bi_2O_3. Besides, the conduction and valence band position of γ-Bi_2O_3 are located at 0.13 and 2.84 V (vs. NHE) [35] and those of $Bi_2Ti_2O_7$ are located at −0.7 and 1.9 V (vs. NHE) [36], providing the suitable thermodynamic energy levels for the possibility of charge separation between them.

Fig. 1 shows the crystalline structure derivation from γ-Bi_2O_3 to $Bi_2Ti_2O_7$ via comparing the structure differentiation along different vector directions. For γ-Bi_2O_3, the structure unit is composed by close packing of [Bi_2O_2] layers, that is the Bi-O tetrahedra units with lattice dimension of 10.25 Å (Fig. 1a). When Ti atoms are incorporated for the formation of $Bi_2Ti_2O_7$, the fragment of structure units is then built by alternately arranged Ti-O octahedra units and Bi-O tetrahedra units with a slight enlarged lattice dimension of 10.37 Å. In this structure, the Ti^{4+} permeated into the lattice originally composed of Bi^{3+} and O^{2-}, and proportional lattice points of metal ion were occupied by Ti^{4+}. Fig. 1b and c clearly display the structure similarities for the derivation from γ-Bi_2O_3 to $Bi_2Ti_2O_7$ from vertical and parallel vector directions, respectively. The detailed structure parameters for both γ-Bi_2O_3 and $Bi_2Ti_2O_7$ can be found in Tables S1 and S2. Due to the similarities in symmetry and crystal lattice between γ-Bi_2O_3 and $Bi_2Ti_2O_7$, it is possibly to fabricate a well-defined heterojunction structure between $Bi_2Ti_2O_7$ and γ-Bi_2O_3 as the co-sharing of Bi-O structure may provide a smooth charge separation pathway across the interface between $Bi_2Ti_2O_7$ and γ-Bi_2O_3.

The different BT/γ-Bi_2O_3 composites were fabricated via a facile in-situ transformation method in hot water bath. γ-Bi_2O_3 was first synthesized and used as the growth substrate to in-situ react with Ti precursors to synthesize BT/γ-Bi_2O_3, in which BT and γ-Bi_2O_3 possess identical cubic symmetry (details in experimental session). The structural and phase transformation for BT/γ-Bi_2O_3 composites were collected by XRD and Raman spectroscopy (Fig. 2). The XRD diffraction peaks at 29.9° and 30.5° (the enlarged part in Fig. 2a) clearly indicate the appearance of $Bi_2Ti_2O_7$ phase (JCPDS No. 32-0118) in BT/γ-Bi_2O_3 composite compared with bare γ-Bi_2O_3 (JCPDS No. 45-1344). Raman characterization (Fig. 2b) further confirms the structural information of BT/γ-Bi_2O_3 samples, in which a Raman band at 148 cm^{-1} is attributed to $Bi_2Ti_2O_7$ in addition to characteristic bands of γ-Bi_2O_3 [37]. The above results clearly indicate that the BT/γ-Bi_2O_3 composite photocatalyst was successfully synthesized using such in-situ transformation method.

Fig. 3a–g displays the mophologies of as-prepared BT/γ-Bi_2O_3 composites with introducing different amount of $Bi_2Ti_2O_7$. Compared to pristine γ-Bi_2O_3 (Fig. 3a), it can be clearly observed that the produced $Bi_2Ti_2O_7$ exhibits nanosheet-like mophology (Fig. 3b–d), which were vertically embedded into γ-Bi_2O_3 substrate and the nanosheets perpendicular to each other with their thickness is about 10 nm, forming a hierarchical structure. It should be emphasized that the embedded $Bi_2Ti_2O_7$ nanosheets have a very close contact with the γ-Bi_2O_3 substrate as the $Bi_2Ti_2O_7$ were in-situ transformed from γ-Bi_2O_3 and Ti precursor under high-temperature water bath condition. The resulted hierarchical structure built by $Bi_2Ti_2O_7$ nanosheets were gradually increased with increasing the amount of Ti precursors (Fig. 3e–g). Such

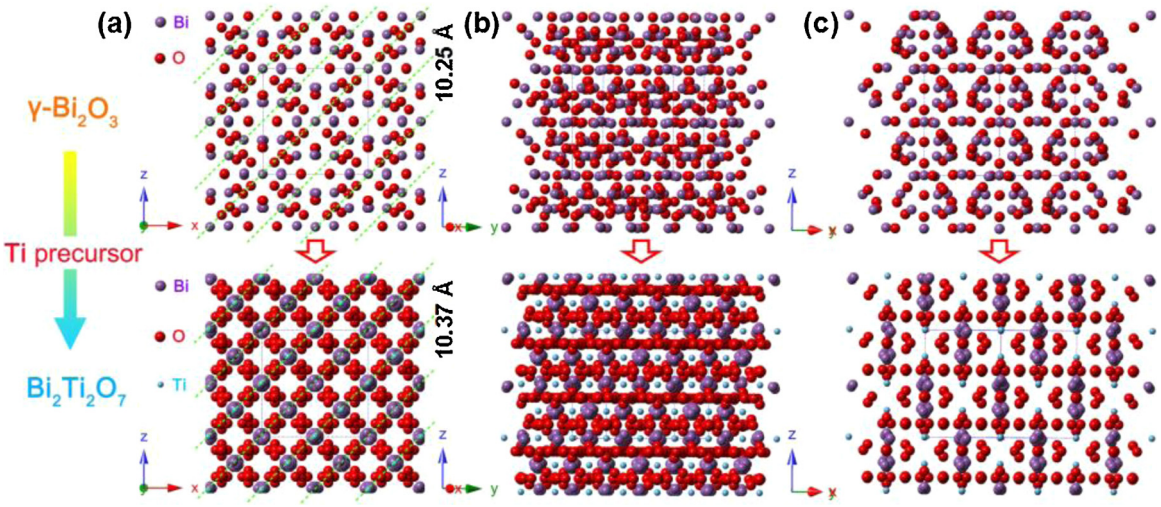

Fig. 1. Crystalline structure derivation from γ-Bi_2O_3 to $Bi_2Ti_2O_7$.

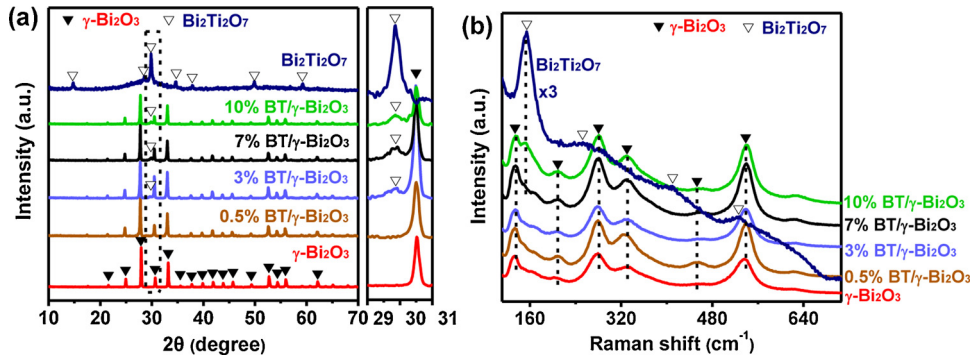

Fig. 2. (a) XRD patterns and (b) Raman spectra of γ-Bi_2O_3, $Bi_2Ti_2O_7$, and BT/γ-Bi_2O_3 composites.

unique hierarchical structure between γ-Bi_2O_3 and $Bi_2Ti_2O_7$ may possess many advantages, e.g., it is possibly benifit the transport of photogenerated charge carriers along the axial γ-Bi_2O_3 and the radical $Bi_2Ti_2O_7$ directions, which enables the spatial charge separation. To clearly understand the process of in-situ transformation for BT/γ-Bi_2O_3 composite with hierarchical structure, a schematic description of such process can be illustrated in Fig. 3h.

To investigate the as-prepared BT/γ-Bi_2O_3 heterojunction with hierarchical structure is possible for promoting spatial charge separation or not, the energy levels for as-prepared $Bi_2Ti_2O_7$ and γ-Bi_2O_3 were first examined using UV–vis absorption and Mott-Schottky characterizations (Fig. 4a–c). The results from Fig. 4a and b revealed that $Bi_2Ti_2O_7$ and γ-Bi_2O_3 exhibit the absorption band edges at around 449 and 520 nm, corresponding to the estimated band gaps (E_g) of 2.96 and 2.66 eV, respectively, which are in good agreement with that reported by Kudo et al. [38] and Yao et al. [39]. The estimated conduction band levels for both $Bi_2Ti_2O_7$ and γ-Bi_2O_3 can be calculated from their Mott-Schottky curves as shown in Fig. 4c, and the minimum conduction band (CB) levels for γ-Bi_2O_3 and $Bi_2Ti_2O_7$ are located at 0.02 and −0.34 eV, respectively. Therefore, the maximum valence band (VB) positions for γ-Bi_2O_3 and $Bi_2Ti_2O_7$ are present at 2.68 and 2.62 eV, respectively.

The band energy levels for γ-Bi_2O_3 and $Bi_2Ti_2O_7$ can be schematically depicted in Fig. 4e, as discussed above, the CB position of γ-Bi_2O_3 is positive than that of $Bi_2Ti_2O_7$ while the VB level of $Bi_2Ti_2O_7$ is negative than of $Bi_2Ti_2O_7$. When considering from the thermodynamic requirement, such band aliment of γ-Bi_2O_3 and $Bi_2Ti_2O_7$ can provide a suitable driven force for the separation of photogenerated charge carriers, i.e., the photo-generated electrons on $Bi_2Ti_2O_7$ can be transferred to the γ-Bi_2O_3 while holes migrate to the opposite side (Fig. 4e). To verify the efficient charge separation can take place at the interface

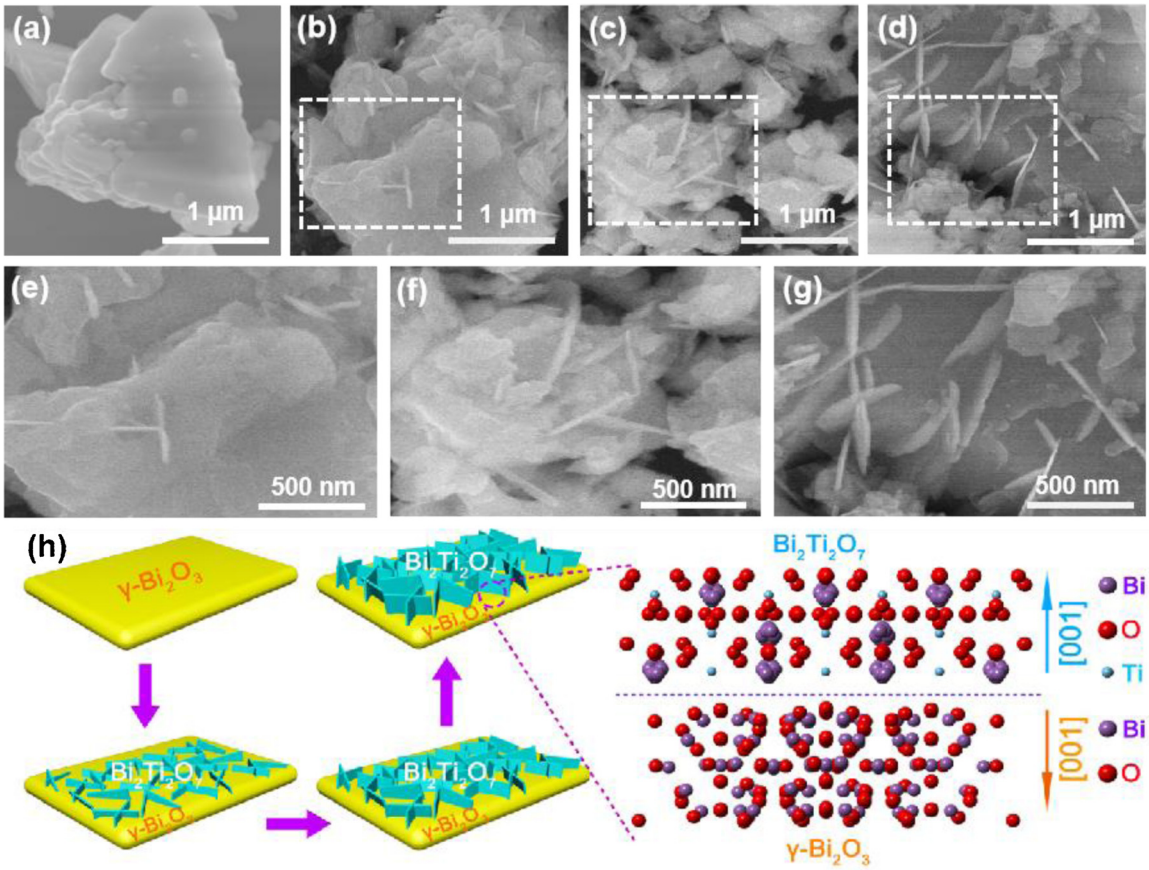

Fig. 3. SEM images of (a) γ-Bi_2O_3, (b, e) 0.5% BT/γ-Bi_2O_3, (c, f) 3% BT/γ-Bi_2O_3, and (d, g) 7% BT/γ-Bi_2O_3. (h) The schematic illustration of the preparation process of the preparation process for the BT/γ-Bi_2O_3.

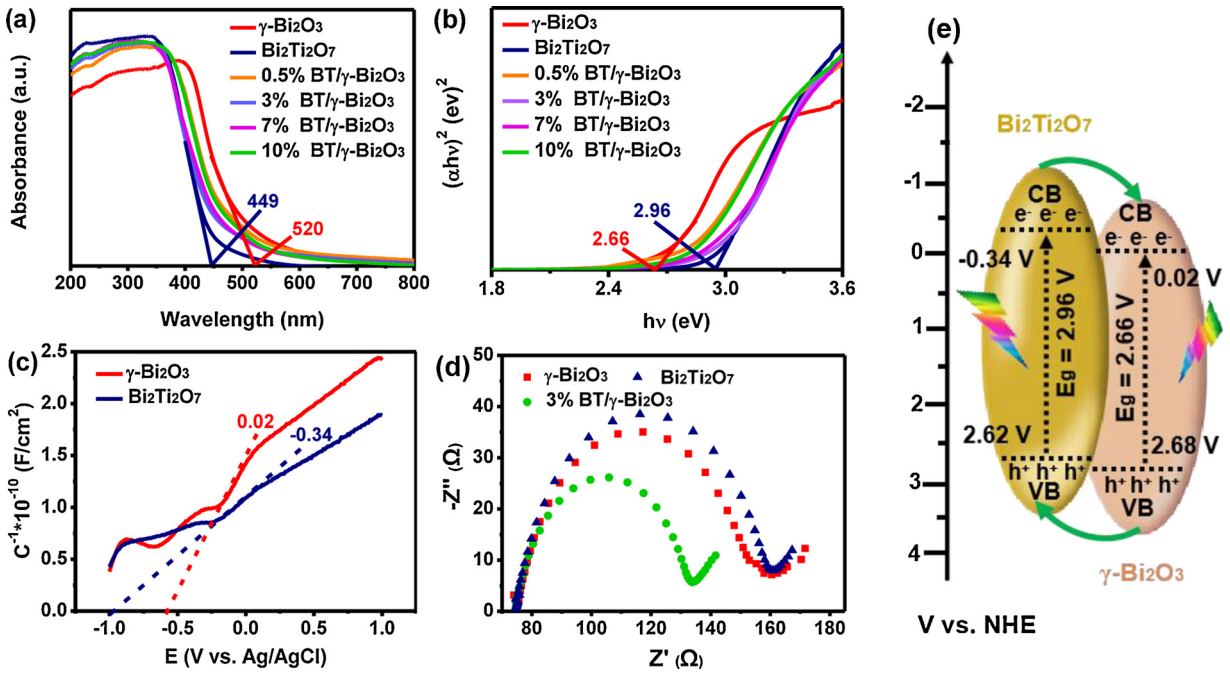

Fig. 4. (a) UV–vis DRS and (b) Tauc's plots of γ-Bi_2O_3, $Bi_2Ti_2O_7$, and BT/γ-Bi_2O_3 samples. (c) Mott-Schottky plots of γ-Bi_2O_3 and $Bi_2Ti_2O_7$ (the inset values are potentials versus Reversible Hydrogen Electrode, RHE). (d) The proposed charge separation and transfer pathways on BT/γ-Bi_2O_3. d) EIS plots of γ-Bi_2O_3 and BT/γ-Bi_2O_3. (e) Energy level diagram of $Bi_2Ti_2O_7$ and γ-Bi_2O_3.

between γ-Bi_2O_3 and $Bi_2Ti_2O_7$, electrochemical impedence spectroscopy (EIS) was employed (Fig. 4d). The results showed that the arc radius of the BT/γ-Bi_2O_3 with heterojunction was much smaller than that of bare γ-Bi_2O_3 and $Bi_2Ti_2O_7$, that is, the BT/γ-Bi_2O_3 composite possesses a lower charge separation resistant than single composite, suggesting that there exists a charge separation and transfer process between the interface of $Bi_2Ti_2O_7$ and γ-Bi_2O_3 [40,41]. Such efficient charge separation is proposed to be attributable to the co-sharing of Bi-O tetrahedra units between $Bi_2Ti_2O_7$ and γ-Bi_2O_3 in heterojunction structures, which provides an atomic charge transferring pathway for the separation of photogenerated charge carriers.

To demonstrate the effect of well-defined heterojunction for spatial charge separation and the contribution to photocatalytic reactions, we chose photocatalytic removal of environmental pollutants with high concentration as model reactions. As the dramatic increasing concern for environmental issue nowadays, the removal of environmental pollutants, especially for high concentration pollutants have become one of the key challenges [2]. Several typical pollutants including dyes, phenol, and sulfur containing compounds are commonly present in the wastewater from dye industries and petroleum refinery [42]. We then chose four model pollutants respective from dyes, phenol, and sulfur containing compounds, rhodamine B (RhB), methyl orange (MO), 4-chlorophenol (4-CP), and dibenzothiophene (DBT) as examples, and the initial concentration of all these compounds was fixed to 20 mg/L.

As depicted in Fig. 5, γ-Bi_2O_3 shows negligible photocatalytic activity (< 5%) for the photodegradation of all these compounds (Figs. S1–S4) and the corresponding constant rate k is calculated to be less than 0.05 min^{-1}. Nevertheless, the photocatalytic degradation activity of γ-Bi_2O_3 can be remarkably enhanced to more than two orders when a very small amount of $Bi_2Ti_2O_7$ was fabricated on the surface. The photocatalytic activities were further improved with increasing the amount of $Bi_2Ti_2O_7$ and the optimized photocatalytic performance can be achieved at ~3% for the degradation of all the four compounds. For the reaction rates on BT/γ-Bi_2O_3 compared with bare γ-Bi_2O_3, the enhancements exceed more than 381 times, 2003 times, 15 times and 20 times for the degradation of RhB (Fig. 5a), MO (Fig. 5b), 4-CP (Fig. 5c), and DBT (Fig. 5d) respectively. Notably that the photocatalytic degradation conversions of all these cases can reach nearly 100% in less than 1 h. As a comparison, blank experiments indicate that no appreciable degradation is detected in the absence of light irradiation or photocatalyst, suggesting that all these compounds were degraded by a photocatalytic reaction of the photocatalyst. To make the result more reasonable, the rate constant k was normalized by specific surface area (Table S3, k/S_{BET}) [43], and the corresponding results exhibit a very similar trend with the rate constant k. This implies that the surface area is not the main reason for the boosts of photocatalytic activity on the BT/γ-Bi_2O_3 samples than $Bi_2Ti_2O_7$ and γ-Bi_2O_3.

The advantages of such BT/γ-Bi_2O_3 heterojunction were further confirmed when comparing with the physical mixture sample (pure γ-Bi_2O_3 and $Bi_2Ti_2O_7$ powder were ground and mixed together, denoted as 3% BT + γ-Bi_2O_3), which only shows a comparable photocatalytic activity with bare $Bi_2Ti_2O_7$ or γ-Bi_2O_3 (Fig. 5). This result may be due to the poor contact between $Bi_2Ti_2O_7$ and γ-Bi_2O_3 in physical mixture sample, which does not allow efficient charge separation between $Bi_2Ti_2O_7$ and γ-Bi_2O_3. However, $Bi_2Ti_2O_7$ nanosheets are in-situ grown from γ-Bi_2O_3 in BT/γ-Bi_2O_3 to fabricate an atomic charge transferring pathway for spatial charge separation, and consequently contribute for the superior photocatalytic performances.

Furthermore, the long-term stability test of the BT/γ-Bi_2O_3 photocatalyst with hierarchical structure was also performed. As displayed in Figs. 6 and S, the BT/γ-Bi_2O_3 composite shows a very stable behavior after more than 5 cycles, suggesting its superior stability in different pollutants with high concentration [44,45]. These results explicitly demonstrate that the BT/γ-Bi_2O_3 photocatalyst with hierarchical structure is a promising candidate in the potential applications in photocatalytic removal of environmental pollutions.

To better understand the reaction mechanism, the trapping experiments were carried out to identify the active species in photocatalyic reactions on BT/γ-Bi_2O_3 (Fig. 7). The photocatalytic degradation activity was slightly suppressed by the addition of $^{\cdot}OH$ scavenger, whereas the addition of h^+ and $^{\cdot}O_2^-$ scavenger significantly suppressed the photocatalytic performance. This suggests that $^{\cdot}O^{2-}$ and h^+ are possibly participated in the process of photocatalytic degradation reactions on the BT/γ-Bi_2O_3.

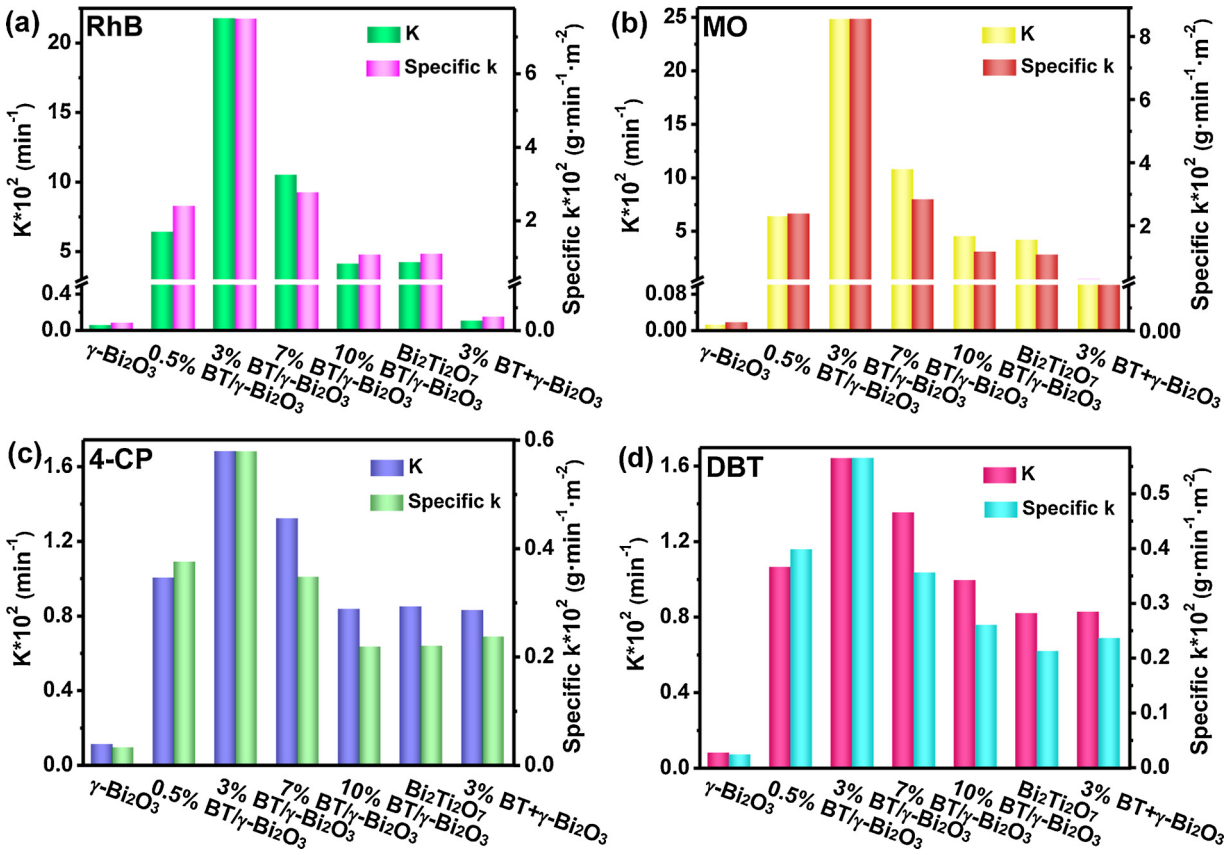

Fig. 5. Apparent rate constants (k) and the rate constants k was normalized by specific surface area (k/S_{BET}) on the photocatalytic degradation of a) RhB, b) MO, c) 4-CP, and d) DBT for γ-Bi_2O_3, BT/γ-Bi_2O_3, and $Bi_2Ti_2O_7$ samples.

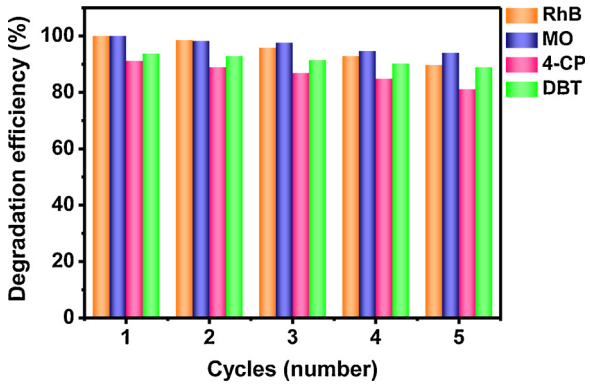

Fig. 6. Stability of degradation of RhB, MO, 4-CP, and DBT on 3% BT/γ-Bi_2O_3.

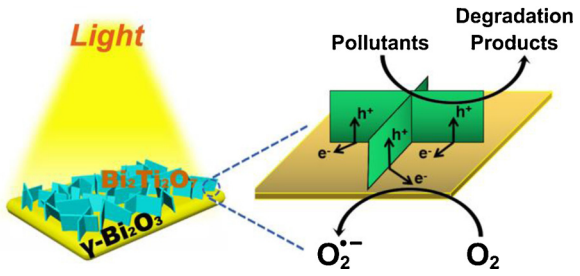

Fig. 8. Schematic illustration of photogenerated charge sepearation in BT/γ-Bi_2O_3.

Based on the above results, the as-prepared BT/γ-Bi_2O_3 heterojunction photocatalyst with hierarchical structure exhibits extremely high photocatalytic activity. The reasons can be ascribed to the following aspects as shown in Fig. 8. For one thing, the similarity of the

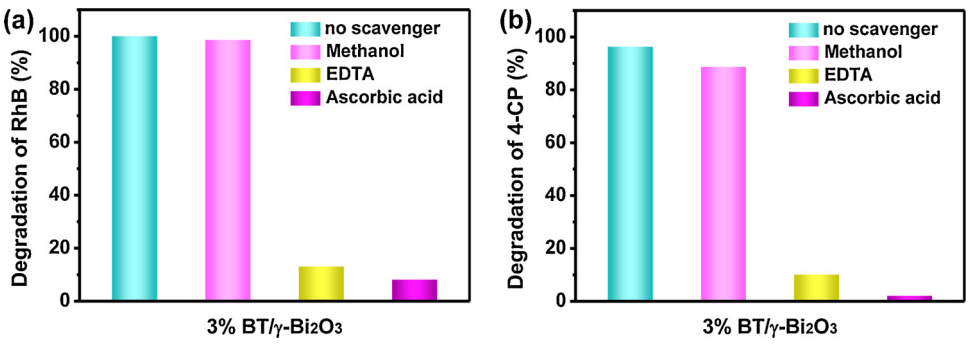

Fig. 7. Trapping experiments of photocatalyic reactions of (a) RhB and (b) 4-CP on 3% BT/γ-Bi_2O_3.

structure and the co-sharing of Bi-O tetrahedra units between $Bi_2Ti_2O_7$ and γ-Bi_2O_3 and in-situ transformation method enable the formation of an atomic charge transferring pathway for spatial charge separation. For another, the formed hierarchical structures benefit the separation of electrons and holes migrate perpendicular to different composites, which is favor of the charge transportation and the following surface reaction process. The performance of $Bi_2Ti_2O_7$ or Bi_2O_3 photocatalyst for organic pollutants removal are listed in Table S4. From Table S2, BT/γ-Bi_2O_3 displayed greater photocatalytic capability for organic pollutants removal among the related materials [39,42,46–49].

4. Conclusion

In conclusion, we have designed and fabricated a hierarchical heterojunction structure between $Bi_2Ti_2O_7$ and γ-Bi_2O_3 (BT/γ-Bi_2O_3) by an in situ transformation method. The BT/γ-Bi_2O_3 hierarchical structures exhibited extremely high photocatalytic activities in photocatalytic removal of various high concentration environmental pollutants, e.g., phenol, dyes, and sulfur containing compounds. The similarity in symmetry of crystal structure and elemental composition of γ-Bi_2O_3 and $Bi_2Ti_2O_7$ created an compact interface favorable for charge separation and transfer, which is due to the co-sharing of Bi-O tetrahedra units for the composites in heterojunction structures to provide an atomic charge transferring pathway for facilitating the spatial charge separation. This work provides an effective strategy for facilitate spatial charge separation and transfer pathway by combining the advantages of hierarchical structure and heterojunction in semiconductor-based photocatalysts for photocatalytic solar energy conversion.

Acknowledgements

This work was supported by the National Natural Science Foundation of China (21573101), the support plan for Distinguished Professor of Liaoning Province ([2015]153), Liaoning BaiQianWan Talents program ([2017]96), the University innovation talent support plan of Liaoning Province (LR2017011), the fund of the State Key Laboratory of Catalysis in DICP (N-15-10). and the Strategic Priority Research Program of Chinese Academy of Sciences (XDA21010207). The author would also like to thank the support from Youth Innovation Promotion Association of Chinese Academy of Sciences and the R&D department of PetroChina.

Appendix A. Supplementary data

Supplementary material related to this article can be found, in the online version, at doi:https://doi.org/10.1016/j.apcatb.2019.02.050.

References

[1] C.R. Lhermitte, B.M. Bartlett, Acc. Chem. Res. 49 (2016) 1121–1129.
[2] M. Iqbal, T.K. Purkait, G.G. Goss, J.R. Bolton, M. Gamal El-Din, J.G.C. Veinot, ACS Nano 10 (2016) 5405–5412.
[3] J.-W. Jang, D. Friedrich, S. Müller, M. Lamers, H. Hempel, S. Lardhi, Z. Cao, M. Harb, L. Cavallo, R. Heller, R. Eichberger, R. van de Krol, F.F. Abdi, Adv. Energy Mater. 7 (2017) 1701536–1701546.
[4] H.-R. An, S.Y. Park, J.Y. Huh, H. Kim, Y.-C. Lee, Y.B. Lee, Y.C. Hong, H.U. Lee, Appl. Catal. B: Environ. 211 (2017) 126–136.
[5] C.M. Ding, J.Y. Shi, Z.L. Wang, C. Li, ACS Catal. 7 (2017) 675–688.
[6] Y. Ao, K. Wang, P. Wang, C. Wang, J. Hou, Appl. Catal. B: Environ. 194 (2016) 157–168.
[7] Y. Bai, L. Ye, L. Wang, X. Shi, P. Wang, W. Bai, P.K. Wong, Appl. Catal. B: Environ. 194 (2016) 98–104.
[8] P. Chen, L. Chen, Y. Zeng, F. Ding, X. Jiang, N. Liu, C.-T. Au, S.-F. Yin, Appl. Catal. B: Environ. 234 (2018) 311–317.
[9] Y.X. Deng, M.Y. Xing, J.L. Zhang, Appl. Catal. B: Environ. 211 (2017) 157–166.
[10] Y. Xu, C. Cheng, S.C. Du, J.Y. Yang, B. Yu, J. Luo, W.Y. Yin, E.P. Li, S.R. Dong, P.D. Ye, X.F. Duan, ACS Nano 10 (2016) 4895–4919.
[11] J.W. Fu, J.G. Yu, C.J. Jiang, B. Cheng, Adv. Energy Mater. 8 (2018) 1701503–1701533.
[12] R.J. Feng, W.Y. Lei, X.Y. Sui, X.F. Liu, X.Y. Qi, K. Tang, G. Liu, M.H. Liu, Appl. Catal. B: Environ. 238 (2018) 444–453.
[13] W.J. Wang, G.Y. Li, T.C. An, D.K.L. Chan, J.C. Yu, P.K. Wong, Appl. Catal. B: Environ. 238 (2018) 126–135.
[14] K. Li, M. Han, R. Chen, S.L. Li, S.L. Xie, C. Mao, X. Bu, X.L. Cao, L.Z. Dong, P. Feng, Y.Q. Lan, Adv. Mater. 28 (2016) 8906–8911.
[15] Z.X. Zeng, H.T. Yu, X. Quan, S. Chen, S.S. Zhang, Appl. Catal. B: Environ. 227 (2018) 153–160.
[16] X. Fan, M.-L. Zhang, I. Shafiq, W.-J. Zhang, C.-S. Lee, S.-T. Lee, Adv. Mater. 21 (2009) 2393–2396.
[17] J.Y. Hu, S.S. Zhang, Y.H. Cao, H.J. Wang, H. Yu, F. Peng, ACS Sustain. Chem. Eng. 6 (2018) 10823–10832.
[18] Y. Bai, H. Yu, Z. Li, R. Amal, G.Q. Lu, L. Wang, Adv. Mater. 24 (2012) 5850–5856.
[19] J.Q. Xu, X.D. Li, Z.Y. Ju, Y.F. Sun, X.C. Jiao, J. Wu, C.M. Wang, W.S. Yan, H.X. Ju, J.F. Zhu, Y. Xie, Angew. Chem. Int. Ed. (2018), https://doi.org/10.1002/anie.201807332.
[20] Z.P. Chen, K.W. Mou, X.H. Wang, L.C. Liu, Angew. Chem. Int. Ed. 57 (2018) 1–6.
[21] J. Zhu, F.T. Fan, R.T. Chen, H.Y. An, Z.C. Feng, C. Li, Angew. Chem. Int. Ed. 54 (2015) 9111–9114.
[22] C.L. Yu, Z. Wu, R.Y. Liu, D.D. Dionysiou, K. Yang, C.Y. Wang, H. Liu, Appl. Catal. B: Environ. 209 (2017) 1–11.
[23] J. Tian, Y. Sang, G. Yu, H. Jiang, X. Mu, H. Liu, Adv. Mater. 25 (2013) 5075–5080.
[24] J. Li, G.M. Zhan, Y. Yu, L.Z. Zhang, Nat. Commun. 7 (2016) 11480.
[25] Y. Long, Q. Han, Z.Q. Yang, Y.J. Ai, S.A. Sun, Y. Wang, Q.L. Liang, M.Y. Ding, J. Mater. Chem. A 6 (2018) 13005–13011.
[26] J.Q. Li, H. Yuan, Z.F. Zhu, Appl. Surf. Sci. 385 (2016) 34–41.
[27] T. Xiong, M.Q. Wen, F. Dong, J.Y. Yu, L.L. Han, B. Lei, Y.X. Zhang, X.S. Tang, Z.G. Zang, Appl. Catal. B: Environ. 199 (2016) 87–95.
[28] M.Z. Xie, X.D. Fu, L.Q. Jing, P. Luan, Y.J. Feng, H.G. Fu, Adv. Energy Mater. 4 (2014) 1300995–1301000.
[29] X.C. Meng, Z.S. Zhang, J. Mol. Catal. A: Chem. 423 (2016) 533–549.
[30] W. Li, Y. Tian, P.T. Li, B.L. Zhang, H.P. Zhang, W.C. Geng, Q.Y. Zhang, RSC Adv. 5 (2015) 48050–48059.
[31] J. Cao, B.Y. Xu, B.D. Luo, H.L. Lin, S.F. Chen, Appl. Surf. Sci. 257 (2011) 7083–7089.
[32] C.D. Song, X. Wang, J. Zhang, X.B. Chen, C. Li, Appl. Surf. Sci. 425 (2017) 788–795.
[33] Y.R. Su, C.H. Ding, Y.L. Dang, H. Wang, L.Q. Ye, X.L. Jin, H.Q. Xie, C. Liu, Appl. Surf. Sci. 346 (2015) 311–316.
[34] A.L. Hector, S.B. Wiggin, J. Solid State Chem. 177 (2004) 139–145.
[35] Y.Y. Li, J.S. Wang, H.C. Yao, L.Y. Dang, Z.J. Li, Catal. Commun. 12 (2011) 660–664.
[36] B. Allured, S. Delacruz, T. Darling, M.N. Huda, V. Subramanian, Appl. Catal. B: Environ. 144 (2014) 261–268.
[37] S.J. Henderson, O. Shebanova, A.L. Hector, P.F. McMillan, M.T. Weller, Chem. Mater. 19 (2007) 1712–1722.
[38] A. Kudo, S. Hijii, Chem. Lett. 10 (1999) 1103–1104.
[39] W.F. Yao, H. Wang, X.H. Xu, J.T. Zhou, X.N. Yang, Y. Zhang, S.X. Shang, Appl. Catal. A 259 (2004) 29–33.
[40] F.L. Formal, K. Sivula, M. Grätzel, J. Phys. Chem. C 116 (2012) 26707–26720.
[41] M. Sachsenhauser, I.D. Sharp, M. Stutzmann, J. Phys. Chem. C 120 (2016) 6524–6533.
[42] Z.F. Bian, Y.N. Huo, Y. Zhang, J. Zhu, Y.F. Lu, H.X. Li, Appl. Catal. B: Environ. 91 (2009) 247–253.
[43] Y.S. Li, Z.L. Tang, J.Y. Zhang, Z.T. Zhang, Appl. Catal. B: Environ. 207 (2017) 207–213.
[44] Z.Y. Zhang, D.L. Jiang, C.S. Xing, L.L. Chen, M. Chen, M.Q. He, Dalton Trans. 44 (2015) 11582–11591.
[45] Y.C. Huang, W.J. Fan, B. Long, H.B. Li, F.Y. Zhao, Z.L. Liu, Y.X. Tong, H.B. Ji, Appl. Catal. B: Environ. 185 (2016) 68–76.
[46] J. Yi, X. Yuan, H. Wang, H. Yu, F. Peng, Mater. Des. 86 (2015) 152–155.
[47] B. Liu, Q. Mo, J. Zhu, Z. Hou, L. Peng, Y. Tu, Q. Wang, Nanoscale Res. Lett. 11 (2016) 391.
[48] H. Shi, H. Tan, W.-b. Zhu, Z. Sun, Y. Ma, E. Wang, J. Mater. Chem. A 3 (2015) 6586–6591.
[49] T. Selvamani, S. Anandan, L. Granone, D.W. Bahnemann, M. Ashokkumar, Mater. Chem. Front. 2 (2018) 1664–1673.